Science of Remote Sensing 2 (2020) 100007

Contents lists available at ScienceDirect

Science of Remote Sensing

journal homepage: www.journals.elsevier.com/science-of-remote-sensing

Full Length Article

On the outstanding need for a long-term, multi-decadal, validated and quality assessed record of global burned area: Caution in the use of Advanced Very High Resolution Radiometer data

L. Giglio [a,*], D.P. Roy [b]

[a] Department of Geographical Sciences, University of Maryland, College Park, MD, 20742, USA
[b] Center for Global Change and Earth Observations, and Department of Geography, Environment, & Spatial Sciences, Michigan State University, East Lansing, MI, 48824, USA

ARTICLE INFO

Keywords:
Long term
Burned area
Fire
AVHRR
FireCCILT10

ABSTRACT

A long-term, multi-decadal, record of global burned area is needed to understand the interplay between human activity and climate change on fire occurrence and behavior. At present, the longest consistent satellite-based record has been provided by the Moderate Resolution Imaging Spectroradiometer (MODIS) on-board NASA's Terra and Aqua satellites. A long-standing objective within the remote sensing community has been to compile a long-term record of pre-MODIS global fire activity using data acquired with the older Advanced Very High Resolution Radiometer (AVHRR). The recent production and release of one such new data set – the AVHRR-based FireCCILT10 burned area product generated under the auspices of ESA's Climate Change Initiative (CCI) – warrants a fresh consideration of the practical issues confounding the use of AVHRR observations. Here we compare the new 36-year FireCCILT10 product with the AVHRR Long Term Data Record (LTDR) input data used to generate the data set. Despite its recent provenance, we found significant temporal artifacts in the first half, and in the last year, of the FireCCILT10 burned area record, that we show are associated with the orbit drift of the NOAA polar orbiting satellites on which the AVHRR sensor suite resides. Based on these findings, and having noted similar but previously unacknowledged artifacts in two older long-term AVHRR burned area products, we formulate several practical recommendations with respect to use of the FireCCILT10 data set and the development of future long-term AVHRR-based fire data sets. The paper findings reinforce the ongoing need for a long-term, multi-decadal, validated and quality assessed, record of global burned area.

1. Introduction

We are in an era with significant opportunities provided by new terrestrial remote sensing systems, such as the Sentinel satellite series (Malenovský et al., 2012) and spaceborne active remote sensing systems (Dubayah et al., 2020), combined with significant satellite data processing advances provided by inexpensive high performance and cloud computing solutions. Meanwhile, there is a long term archive of satellite data that are difficult to use, and so have been relatively underutilized, but critically were acquired from the 1970's onwards and capture a period through the present when the global human population has more than doubled and evidence for climate change became readily discernible (Roy et al., 2014). The Advanced Very High Resolution Radiometer (AVHRR) sensor series have been in operation from 1978 on the TIROS-N satellite, followed in 1981 on the NOAA Polar Orbiting Environmental Satellite (POES) series, and provide global daily coverage at coarse spatial resolution (Cracknell, 1997).

Fire is recognized as an important process in the terrestrial carbon cycle and increasingly as an indicator of climate change. Satellite remotely sensed fire information is critical for understanding the role of fire in the Earth system. In particular, long term global fire records are needed to understand the interplay between human activity and climate change on fire occurrence and behavior. There is considerable inter-annual variation in fire (Boschetti and Roy, 2008; Giglio et al., 2010) driven predominantly by precipitation, that influences fuel accumulation and the incidence of dry conditions needed for fires to ignite and spread (Chikamoto et al., 2017; Abatzoglou et al., 2018). Phenomena such as the El Niño–Southern Oscillation (ENSO) affect precipitation and temperatures in regionally

* Corresponding author.
E-mail address: lgiglio@umd.edu (L. Giglio).

https://doi.org/10.1016/j.srs.2020.100007
Received 29 February 2020; Received in revised form 25 June 2020; Accepted 16 July 2020
Available online 26 July 2020

different ways and have been shown to affect fire (Alencar et al., 2006; Chen et al., 2017) and occur at irregular near-decadal intervals (Wang et al., 2009; Feng and Tung, 2020). Changes in human population density and land use occur at different time scales and mediate fire by changing ignitions (that can be purposeful or due to accident or arson) and by changing the available fuel load (Archibald et al., 2009; Balch et al., 2017; Bowman et al., 2017). A validated long-term, multi-decadal, satellite-derived record of global burned area is a core goal established in the context of the international global observing system (GCOS/GTOS, 1997; GCOS, 2011) that was redefined by the Committee on Earth Observation Satellites (CEOS) and the Global Climate Observing System (GCOS) to meet the needs of the U.N. Framework Convention on Climate Change (GCOS, 2006; GCOS, 2011).

At present, the longest consistent satellite-based burned area record has been provided by the Moderate Resolution Imaging Spectroradiometer (MODIS) on-board NASA's Terra spacecraft, one of multiple missions comprising NASA's Earth Observing System (EOS). The launch of the MODIS on the Terra and Aqua satellites in 1999 and 2002 enabled, for the first time, systematic production of high quality, multi-year, global 1-km active fire detection and 500-m global burned area products (Justice et al., 2002) that have been reprocessed multiple times to reflect improved algorithms and refined sensor calibration and geolocation knowledge (Giglio et al., 2016, 2018). Long-term fire studies over broad spatial scales are often only defined over the last two decades to the beginning of the MODIS record. Although the most recent Global Fire Emissions Database (GFED4) extends the global burned area record an additional four years into the past (to mid-1996), the data set during those years relies heavily on a burned area climatology and so is less reliable (Giglio et al., 2013).

MODIS was designed to support the needs of the global change science and applications community with a heritage based on the Landsat and AVHRR sensors (Justice et al., 1998). Landsat provides the longest terrestrial satellite record, starting with Landsat 1 data in 1972, but only with sparse global coverage and the most recent Landsat 8 launched in 2013 has a nominal 16-day repeat cycle (Roy et al., 2014; Wulder et al., 2016). The low Landsat temporal revisit and lack of short- and long-wave thermal bands mean that Landsat sensor data alone are not well suited, respectively, for burned area mapping (Roy et al., 2019) or for active fire detection (Schroeder et al., 2016; Kumar and Roy, 2018). The AVHRR sensors notably provide global daily observation coverage and include reflective and thermal bands that are potentially suitable for fire monitoring (Cracknell, 1997; Csiszar et al., 2013). Consequently, a long-standing objective within the remote sensing community has been to compile a record of pre-MODIS global fire activity using data acquired with the AVHRR. Coupled with the more recent MODIS fire record, and with careful calibration, one could in principle assemble a comprehensive record of global fire activity spanning a period of more than 40 years in duration.

Despite the substantial value of a pre-MODIS, global AVHRR fire record, the production of such a data set with sufficient consistency is confounded by various design features and idiosyncrasies of the AVHRR sensor and the host POES platforms on which it resides. The AVHRR data have high radiometric resolution (10 bits) and global daily coverage, but at a cost of coarse spatial resolution and a small number of bands (Cracknell, 1997). The first version of the AVHRR (termed AVHRR/1) had a four-band configuration and was launched in 1978 on-board the TIROS-N platform and was also on NOAA-6, -8 and -10. It was subsequently improved to a five band configuration (AVHRR/2) with two reflective bands (0.65 and 0.86 μm), a mid-infrared band (3.8 μm) and two thermal infrared bands (10.8 and 11.9 μm), and was first launched on NOAA-7 in 1981, and subsequently on NOAA-9, -11, -12, -13, and -14. The latest AVHRR (AVHRR/3) is a six-band sensor, carrying an additional 1.6 μm band, launched on NOAA-15 in 1998 and on all subsequent NOAA satellites. The AVHRR sensors are in polar orbiting sun-synchronous orbits. None were designed for fire monitoring. Their use is confounded by several factors including the sub-optimal 3 × 5 km effective Global Area Coverage (GAC) image resampling scheme (Justice et al., 1989), problematic and/or inconsistent calibration of the red and near-infrared bands (Gorman and McGregor, 1994; Trishchenko, 2002; Trishchenko et al., 2002), variable and/or ill-behaved saturation of the 3.8 μm band (Setzer and Verstraete, 1994; Csiszar and Sullivan, 2002), poor quality image navigation (Krasnopolsky and Breaker, 1994; Brunel and Marsouin, 2000), and significant sensor orbit drift (McGregor and Gorman, 1994; Privette et al., 1995; Kaufmann et al., 2000; Csiszar et al., 2003). While collectively intolerable by contemporary standards, these factors are a byproduct of the more limited technological capabilities and the comparatively short-term meteorological objectives for the early AVHRR sensors. A number of processing activities were initiated to derive large-area terrestrial AVHRR long term data records. However, to date, this endeavor remains an ongoing area of research. Arguably, there is no definitively processed AVHRR record and those that are publicly available are subject to scientific debate. For example, global comparison of the normalized difference vegetation index (NDVI) derived from four AVHRR long term products indicated inconsistent trends among the four products for nearly half the global land surface (Beck et al., 2011).

The catalog of POES AVHRR limitations notwithstanding, AVHRR GAC, 1.1 km Local Area Coverage (LAC), and High Resolution Picture Transmission (HRPT) data have been used in numerous early studies as a source of fire information (e.g., Flannigan and Vonder Haar, 1986; Matson and Holben, 1987; Scholes et al., 1996; Dwyer et al., 1992; Siegert and Hoffmann, 2000; Stroppiana et al., 2000) including large area burned area products generated using several years of data (Fraser et al., 2000; Sukhinin et al., 2004). Produced as part of these efforts (though never publicly released) were two long-term burned area data sets derived from AVHRR GAC imagery: the 17-year (1982–1999) weekly global burnt surface (GBS) product (Carmona-Moreno et al., 2005), and the 18-year (1981–1999) monthly Pathfinder Land burned area data set for tropical Africa (Riaño et al., 2007a). More recently, the 35 year (1982–2017, excluding 1994) FireCCILT10 global burned area product was generated using AVHRR GAC imagery and publicly released (Otón et al., 2019).

The recent production and release of the FireCCILT10 burned area product warrants a fresh consideration of the practical issues confounding the use of AVHRR time series data. Here we focus specifically on the POES orbit drift, which has long been known to distort long-term time series derived from AVHRR observations (McGregor and Gorman, 1994; Privette et al., 1995; Kaufmann et al., 2000; Csiszar et al., 2003; Giglio, 2007). Orbit drift effects have also been documented for other polar orbiting sun-synchronous sensors including the Système Pour l'Observation de la Terre (SPOT) VEGETATION (Swinnen et al., 2014) and the Landsat 5 Thematic Mapper (Zhang and Roy, 2016; Roy et al., 2020). In this study we compare the FireCCILT10 burned area product (Otón et al., 2019) with the input AVHRR Long Term Data Record (LTDR) data (Pedelty et al., 2007) that were used to generate the FireCCILT10 product. We find significant orbit-drift artifacts in the FireCCILT10 burned area time series. Based on these results, and having noted similar but previously unacknowledged artifacts in the older GBS and Pathfinder burned area data sets, we formulate several practical recommendations with respect to (i) use of the FireCCILT10 data set and (ii) the development of future long term AVHRR-based fire data sets. Following these recommendations, we discuss the ongoing need for a validated and quality assessed, long-term, multi-decadal, record of global burned area.

2. Long-term AVHRR burned area studies and data sets

Several notable long-term, large scale AVHRR burned area products have been produced under separate efforts. They are summarized below. In addition, a number of regional and limited temporal coverage AVHRR burned area products have been generated and are surveyed briefly in Chuvieco et al. (2019).

The first effort generated a weekly 8 km global burnt surface (GBS) product for 17 years (1982–1999) (Carmona-Moreno et al., 2005).

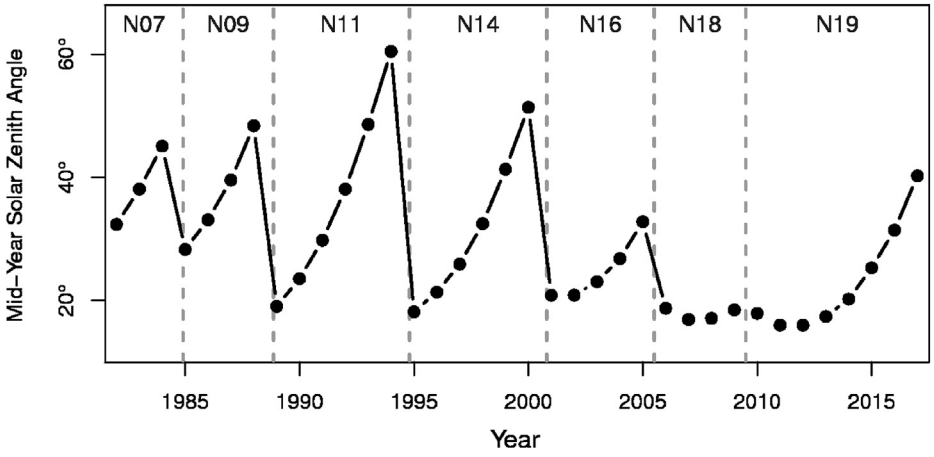

Fig. 1. Mean zonal solar zenith angle over the Tropic of Cancer (23.44°N) on June 21st (summer solstice) for 36 years (1982–2017) derived from the version 5.0 AVHRR Long Term Data Record (LTDR) AVH09C1 0.05° surface reflectance product for the NOAA-7, -9, -11, -14, -16, -18, and -19 afternoon satellites. Dashed vertical lines indicate each transition to a new AVHRR instrument in the LTDR time series. Abbreviated labels N07, N09, etc. denote the NOAA-7, -9, -11, -14, -16, -18, and -19 satellites, respectively.

AVHRR data for four AVHRR sensors processed by the Pathfinder AVHRR Land processing system (Agbu and James, 1994) were used. Atmospherically corrected red and near-infrared (NIR) reflectance and the top-of-atmosphere (TOA) brightness temperature and reflectance retrieved from the 3.8 μm mid-infrared band were used. An additional orbit-degradation correction of the 3.8 μm band was applied that was formulated by examination of the time series over a stable Libyan Desert site (Carmona-Moreno et al., 2005). The efficacy of this correction is questionable since the 3.8 μm band was not designed for hot land-surface monitoring, such as deserts, and saturates at an equivalent blackbody temperature of ~322 K, with saturation varying by up to several kelvins among AVHRR sensors (Csiszar and Sullivan, 2002). The GBS burned area mapping algorithm employed a series of relative- and absolute-threshold tests applied to weekly composites of the red and NIR surface reflectance, the retrieved TOA 3.8 μm reflectance, and two non-linear band indices calculated using different combinations of the red and NIR surface reflectance and the TOA 3.8 μm brightness temperature. The GBS product was not made publicly available.

The second effort generated a monthly, 8 km burned area product encompassing tropical Africa for 18 years (1981–1999) (Riaño et al., 2007a) using the same Pathfinder AVHRR Land data and from the same four AVHRR sensors used to produce the GBS product. However, a more sophisticated orbit-degradation correction was implemented for the 3.8 μm mid-infrared band using sensor-specific lookup tables, with observations acquired during the first year of operation serving as a reference for the remainder of each sensor's operational life. The mapping algorithm for this data set was virtually identical to that used by Carmona--Moreno et al. (2005), with the addition of a relative threshold test applied to the weekly time series of TOA mid-infrared 3.8 μm brightness temperature. This product was also not made publicly available. A subsequent effort by Riaño et al. (2007b) generated a 20-year global burned area data set derived from reconfigured 8-km Pathfinder AVHRR data and was also not publicly released but was used by the authors to investigate spatial and temporal burned area trends.

The most recent effort generated a monthly global 0.05° burned area product for 35 years (1982–2017, excluding 1994) (Otón and Chuvieco, 2018; Otón et al., 2019). The AVHRR data were processed by the NASA Long Term Data Record (LTDR) project (Pedelty et al., 2007), and the most recent Version 5.0 LTDR data were used that include a bidirectional reflectance distribution function (BRDF) correction of the red and NIR bands (Villaescusa-Nadal et al., 2019) that may reduce orbit drift effects in these bands. A total of seven AVHRR sensors were used. A supervised random forest classification approach, using training data derived from eight years of the NASA MODIS burned area product (Giglio et al., 2018) and monthly composites of an AVHRR burned area index defined by the AVHRR red and near-infrared surface reflectance and the 11.9-μm brightness temperature and non-linear spectral band indices of the red and near-infrared, were used. Otón et al. (2019) reported unrealistic changes between consecutive years in the mapped burned area. Despite this caveat, the product, named FireCCILT10, was released to supplement

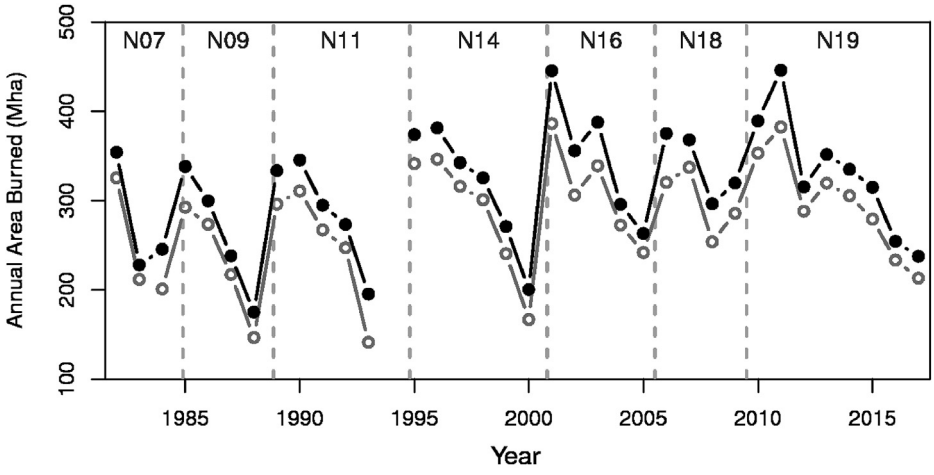

Fig. 2. Global annual area burned defined by the FireCCILT10 product (black line, filled circles) for 35 years (1982–2017, but excluding 1994 when no FireCCILT10 product was generated). The light grey line with open circles shows the annual FireCCILT10 burned area for the tropical zone spanning latitudes 20°S to 20°N, where the greater majority of the global burned area is reported. Satellite annotations are as in Fig. 1.

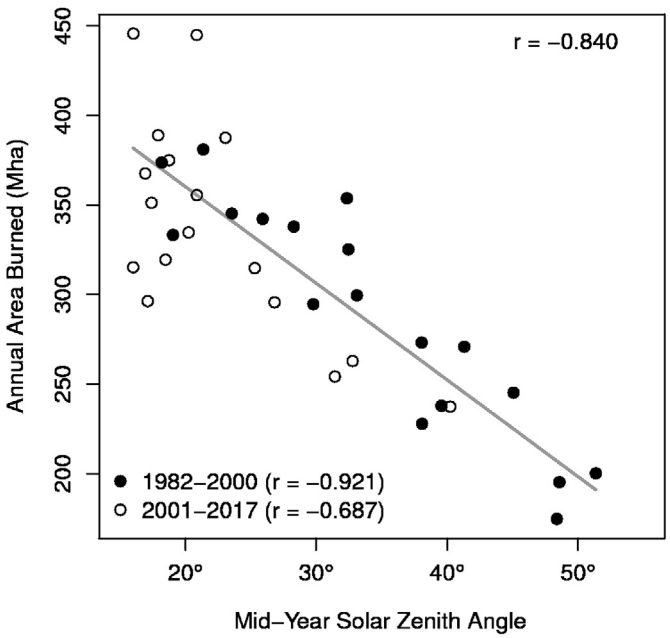

Fig. 3. Scatter plot comparing Figs. 1 and 2 data for the 35 corresponding years of each time series. The grey line shows the fitted Tukey (1977) outlier-resistant regression line. The black and white symbols indicate values from the pre-MODIS (1982–2000) and MODIS-era (2001–2017), respectively, for which the respective linear correlation coefficients (r) are also noted.

a number of other available burned area products generated by the European Space Agency-sponsored Fire Climate Change Initiative (CCI) project (https://www.esa-fire-cci.org/). The data set was upon release in March 2019 designated as a beta version on various project web sites (e.g., https://www.esa-fire-cci.org/FireCCILT) and more recently in the associated product documentation (e.g., Otón et al., 2020).

3. Analysis

3.1. AVHRR orbit drift correlation with annual FireCCILT10 burned area

The FireCCILT10 burned area product is ideal for demonstrating the critical importance of compensating for satellite orbit drift in the production of any long-term AVHRR burned area record. NOAA aims to keep at least two AVHRR satellites in orbit, and because of this requirement and their relatively short five-year sensor design lifetimes, the NOAA orbits are not as strictly maintained as many other environmental remote sensing systems (Ignatov et al., 2004). Consequently, unlike the orbit of a maintained polar orbiting sun-synchronous sensor that is characterized by a constant mean sunlit equatorial crossing time and a local overpass time that changes only with latitude (Wertz, 2001), the AVHRR overpass time changes over the sensor lifetime.

Fig. 1 shows, for each year from 1982 to 2017, the mean solar zenith angle around the Tropic of Cancer (23.44°N) on June 21st (i.e., the summer solstice) for the NOAA-7, -9, -11, -14, -16, -18, and -19 afternoon satellites. For a polar orbiting sun-synchronous sensor in a maintained orbit, the solar zenith angle at the time of overpass is the same at all locations along the same latitude (Zhang et al., 2016). However, the solar zenith angles in Fig. 1 are not constant over time. This variability is due to the NOAA AVHRR orbit drift that changes the local overpass time and so the solar zenith angle. Fig. 1 clearly shows the orbit drift of the successive afternoon NOAA satellites, with the overpass occurring progressively later in the day over the lifetime of each satellite. A later overpass time means that the sun is lower in the sky, with a correspondingly larger solar zenith angle. The significant discontinuities in the solar zenith angle time series with each switch to a new satellite are very pronounced and as great as 42.6° with the transition from NOAA-11 to NOAA-14. The local overpass times of the NOAA morning satellites, e.g., NOAA-10, NOAA-12, etc., drift progressively earlier, but these are not illustrated as they were not used to generate the FireCCILT10 burned area product.

The results in Fig. 1 were derived from the same AVHRR LTDR product that was used to generate the FireCCILT10 burned area product. Fig. 2 shows the global annual area burned reported by FireCCILT10. It is well established that the majority of burning globally occurs in the tropics (Giglio et al., 2013) and this is the case for the FireCCILT10 with 89% of the mapped burning occurring between latitudes 20°S to 20°N considering all 35 product years. However, a disconcerting pattern is evident when Figs. 1 and 2 are compared. There is a significant decline in the reported FireCCILT10 global burned area over the lifetime of each AVHRR sensor, followed by an abrupt and very pronounced increase (typically ~50%) with each transition to a new satellite. The solar-zenith-angle and burned-area time series are anti-correlated. This is evident in Fig. 3 that shows Figs. 1 and 2 data plotted against each other, revealing a significant correlation between the two time series ($r = -0.840$, $p \approx 10^{-10}$).

In Fig. 3 the data for the years before 2001 and for 2001 onwards are shown marked separately. Prior to 2001 the annual FireCCILT10 global burned areas tend to be lower and the solar zenith angles higher. The correspondence between the mapped area burned and the solar zenith angles is greater for 1982–2000 ($r = -0.921$) than for 2001–2017 ($r =$

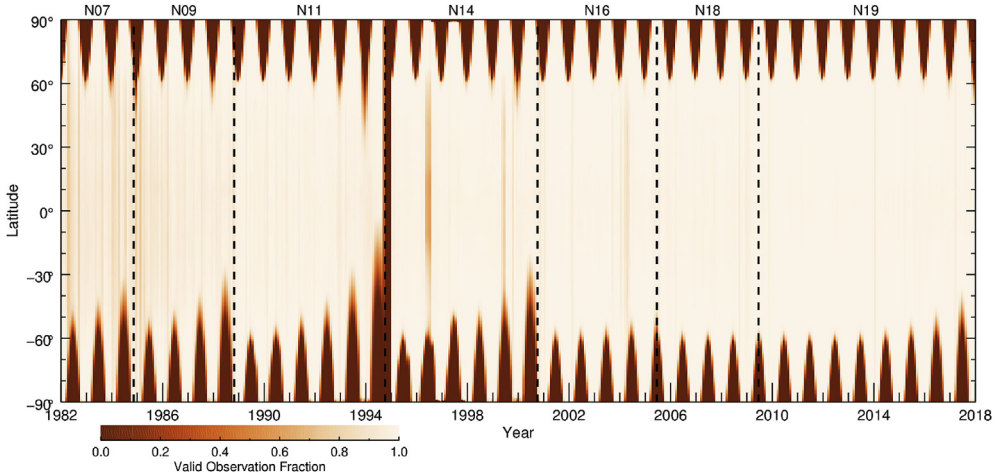

Fig. 4. Hovmöller plot showing the monthly latitudinal fraction of valid LTDR observations for the 36-year AVHRR LTDR time series. Satellite annotations are as in Fig. 1.

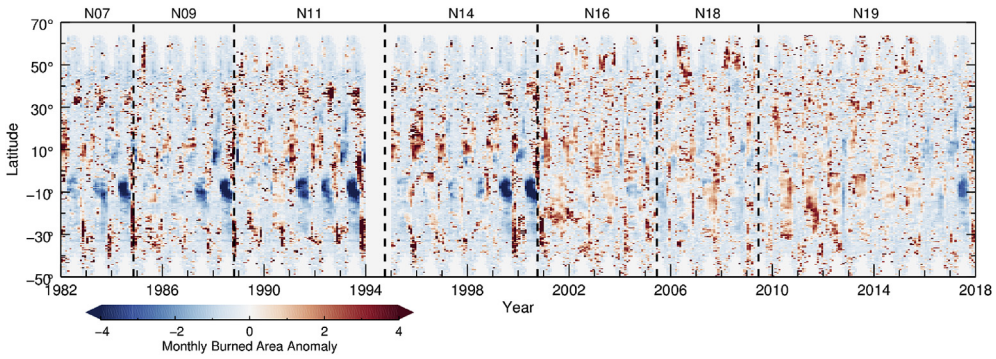

Fig. 5. Hovmöller plot of monthly zonal burned area anomaly (as Z-scores) over the 36-year FireCCILT10 time series, relative to the 2001–2017 climatology. The Z-score is defined as the difference between the area burned in a given month and the 2001–2017 climatological mean burned area for that month, divided by the 2001–2017 climatological burned area standard deviation for that month. Satellite annotations are as in Fig. 1.

−0.687). The earlier 1982–2000 period includes the greatest obit drift and hence the greatest changes in solar zenith angle (Fig. 1). The later period corresponds to the MODIS era and includes years when the MODIS burned area product was used to calibrate the FireCCILT10 algorithm and also when the FireCCILT10 product was considered to exhibit "more stable trends" (Otón et al., 2019) and during which "temporal trends in Tropical regions have been observed more accurate, particularly since 2001" (Otón et al., 2020).

The very high correlations in Fig. 3 between the FireCCILT10 annual area burned and the AVHRR solar zenith angle could be due to several factors. As the FireCCILT10 burned area mapping algorithm is not sufficiently described to be unambiguously duplicated, we examine below non-algorithm factors, namely, (i) the different geographic availability of daylit data sensed by AVHRR sensors, and (ii) changes in the radiometric properties of the AVHRR data, that are both related to changes in the sensor overpass times.

3.2. Analysis of geographic availability of daylit AVHRR time series

Fig. 4 shows a Hovmöller plot, commonly used to summarize global meteorological variables over time in a single figure (Hovmöller, 1949), that illustrates the latitudinal availability of the AVHRR LTDR data. The monthly fraction (0–1) of daily AVHRR observations flagged as valid in the LTDR quality assessment band over each calendar month are shown for the 36 study years. At high latitudes, particularly above the polar circles (latitudes above 66°N and 66° S), there are no valid winter observations because the POES satellite overpass occurs during the night (solar zenith angle > 90°). The evident temporal variation in the "spikes" of missing LTDR data are coupled to the satellite orbit drift as the ascending orbital node occurs progressively later in the day for each NOAA POES "pm" satellite. This results in a shift of the southern limit of available daytime AVHRR observations further northward. Over the 36 year period, different daylit geographic areas are available that could affect AVHRR based burned area mapping.

Fig. 5 shows a Hovmöller plot of the monthly zonal FireCCILT10 burned area anomaly derived relative to the 2001–2017 monthly FireCCILT10 burned area climatology. As evident in Fig. 4, the FireCCILT10 is not defined in the winter months when there were no available daylit valid AVHRR LTDR observations. Several unusual features are apparent in Fig. 5. In particular, prominent negative burned area anomalies occur near 10°S that grow in magnitude over the lifetime of each AVHRR sensor in use prior to 2001, abruptly ending with each transition to a new platform. The early stage of a similar anomaly is also evident in 2017 for the NOAA-19 AVHRR. Before 2001, negative anomalies are also apparent above 5°N and extend for some years up to more than 20°N with a similar evolution over the lifetime of each AVHRR sensor.

In Fig. 5 there are also several minor unusual features, including, for example, narrow (i.e., short duration) positive burned area anomalies near 30°S pre-2001 that increase in amplitude at the NOAA-9, NOAA-11, NOAA-14, and NOAA-16 AVHRR transitions. It is unclear if these anomalies are associated with fewer LTDR observations that occur occasionally around 30°S (Fig. 4) as fewer observations would typically result in burned area mapping omission errors, which would result in negative anomalies rather than the positive anomalies seen in Fig. 5.

The most apparent pre-2001 negative burned area anomalies in Fig. 5 occur near 10°S, and above 5°N, predominantly in the Tropics, i.e., between 20°S and 20°N where the greater majority of all the global FireCCILT10 burned areas were mapped (Fig. 2). Fig. 6 shows the annual FireCCILT10 burned area plotted against the fraction of good LTDR observations for the Tropics (20°S and 20°N), for the non-tropical regions (hereafter referred to as the "extra-tropics"), and for the entire globe. The good LTDR observation criteria used to derived the *x*-axis values in Fig. 6 are the same as those used by (Otón et al., 2019), i.e., LTDR observations "without 'no data values' or reflectance equal to or higher than 90%".

For all the years the plotted data are moderately correlated globally ($r = 0.656$), but are less correlated for the tropics ($r = 0.313$) and the extra-tropics ($r = 0.249$). The global correlations do not change much between the 1982–2000 ($r = 0.622$) and the 2001–2017 ($r = 0.677$) time periods. However, these global correlations include the tropics, where the greater majority of the FireCCILT10 mapped annual burning occurred, and the extra-tropics, where the missing good LTDR observations are most pronounced. Consequently, the correlations are inflated because the tropical FireCCILT10 burned area and the extra-tropical LTDR good-observation fraction are themselves correlated with the solar zenith angle and hence with the AVHRR orbit drift (Figs. 2 and 4). Notably, Fig. 6 correlations change substantially, from almost no correlation for 1982–2000 in the tropics ($r = 0.067$) and the extra-tropics ($r = -0.154$), to much higher correlations for 2001–2017 in the tropics ($r = 0.456$) and the extra-tropics ($r = 0.451$). In the 1982–2000 period the low ($r = 0.067$) tropical correlation equates to only 0.45% ($= r^2$) of the variability in annual burned area explained by the number of good quality LTDR observations available to the mapping algorithm. In contrast, if the variables plotted in Fig. 3 are similarly restricted to the tropics, the tropical FireCCILT10 annual burned area is strongly correlated with the solar zenith for 1982–2000 ($r = -0.926$) and also for 2001–2017 ($r = -0.704$) and all years ($r = -0.860$). Within the tropics, solar zenith angle explains nearly 86% ($= 0.926^2$) of the variability in annual FireCCILT10 burned area during the 1982–2000 period. Evidently, during this period, which includes the greatest orbit drift and hence solar zenith angle changes (Fig. 1), factors other than a lack of good LTDR observations influence the annual tropical FireCCILT10 mapped burned area.

3.3. Analysis of temporal stability of AVHRR time series

Satellite orbit-drift changes the local overpass time and therefore changes in turn (i) the retrieved reflectance over non-Lambertian

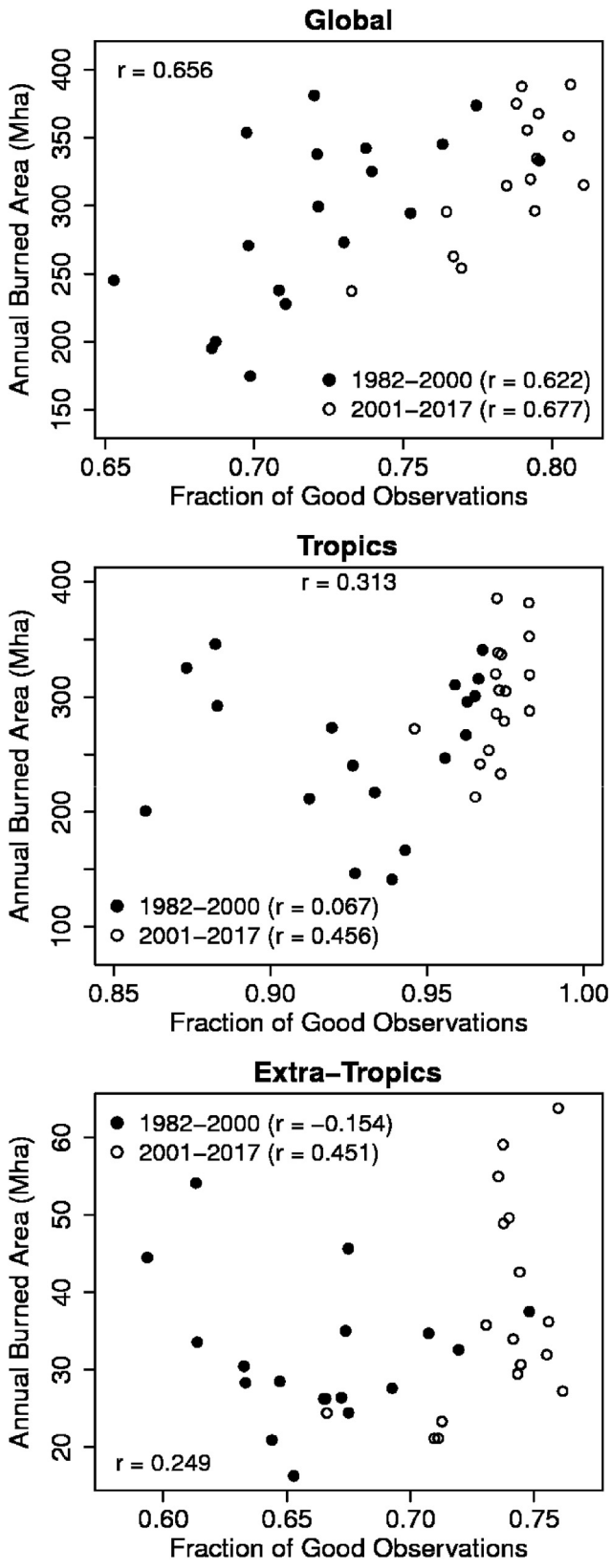

Fig. 6. Annual FireCCILT10 burned area mapped plotted against the fraction of good quality LTDR observations available for each year. The black and white symbols indicate values from the pre-MODIS (1982–2000) and MODIS-era (2001–2017), respectively, for which the respective correlation coefficients (*r*) are also noted. Results are shown for the tropics (latitudes 20°S to 20°N), the extra-tropics (latitudes above 20°N and below 20°S), and globally.

surfaces due to the change in solar zenith at the time of observation (Zhang and Roy, 2016; Roy et al., 2020), and (ii) the observed radiance (or, equivalently, brightness temperature) because of surface diurnal temperature variations (Privette et al., 1995). Figs. 7 and 8 show LTDR monthly 11.9-μm (band 5) brightness temperature (units: kelvins) and atmospherically corrected red and NIR nadir BRDF reflectance (NBAR) (unitless), respectively, for four desert calibration sites. At these desert locations the atmospheric contribution is usually minimal due to the prevailing arid conditions (Cosnefroy et al., 1996). The LTDR AVHRR data are provided as daily gridded data, and in Figs. 7 and 8 monthly composited values are shown. The monthly composites were derived using the maximum 10.8-μm (band 4) brightness temperature criterion which is well established for AVHRR data and tends to preferentially select cloud-free data (Cihlar et al., 1994; Roy, 1997), and was the same criterion used to derive the monthly values used in the FireCCILT10 product generation algorithm (Otón et al., 2019).

Evidently the LTDR processing has not completely removed temporal orbit drift effects. The drift to later afternoon overpass times causes the AVHRR to acquire imagery later in the day, giving the misleading impression that the land surface is growing increasingly cooler over the lifetime of each AVHRR sensor. This is quite apparent for all the desert sites in Fig. 7. The LTDR algorithm does not correct the thermal bands for bidirectional emissivity effects but these are typically small, even over the wide 110° field of view of MODIS or AVHRR (Snyder et al., 1997). Notably, there are clear discontinuities when the data transition between sensors, for example, between NOAA-9 and NOAA-11 and between NOAA-11 and NOAA-14, when the overpass times (and hence solar zenith angles) change markedly (Fig. 1). The same discontinuities are apparent in the red and NIR reflectance (Fig. 8). The atmospherically corrected LTDR data are processed with a bidirectional reflectance distribution function (BRDF) correction of the red and NIR bands to surface nadir BRDF-adjusted reflectance (NBAR) (Villaescusa-Nadal et al., 2019). It is unknown how well this correction performs operationally in minimizing AVHRR directional reflectance effects in space and time and in particular with respect to the large AVHRR solar zenith orbit drift variations. The plotted red and NIR NBAR values in Fig. 8 are very high and spectrally indicative of unvegetated desert locations. However, the NBAR values are not temporally constant and, given that they are for desert sites where surface moisture variation and atmospheric contamination is low, we suspect that the NBAR correction is imperfect. The extent to which the FireCCILT10 statistical normalizations used to compensate for the effects of orbit-drift on the LTDR input data were successful is unclear.

4. Discussion

The results of the preceding analysis demonstrate the presence of significant artifacts in the FireCCILT10 global burned data that arise as a consequence of the NOAA AVHRR satellite orbit drift. Based on these results we also believe that the earlier AVHRR-based GBS (Carmona-Moreno et al., 2005) and Pathfinder Land burned area (Riaño et al., 2007a) products were similarly impacted. Although neither product was publicly released, several figures in the relevant publications show time series artifacts similar to those we found for the FireCCILT10, most notably abrupt jumps in the burned area time series coinciding with each transition to a new NOAA satellite (Carmona-Moreno et al., 2005, cf. Figure 9; Riaño et al. (2007a), cf. Fig. 2). We note also that in the case of Riaño et al. (2007a) the cross- and intra-sensor AVHRR 3.8 μm band calibration they attempted was likely compromised by frequent saturation over hot and/or bright surfaces. Specifically, as we stated earlier, the AVHRR 3.8 μm channel was not designed for hot land-surface monitoring and typically saturated at ~322 K (Csiszar and Sullivan, 2002). Under such conditions at least one measured value is spurious, and no meaningful reconciliation of disparate signals is possible.

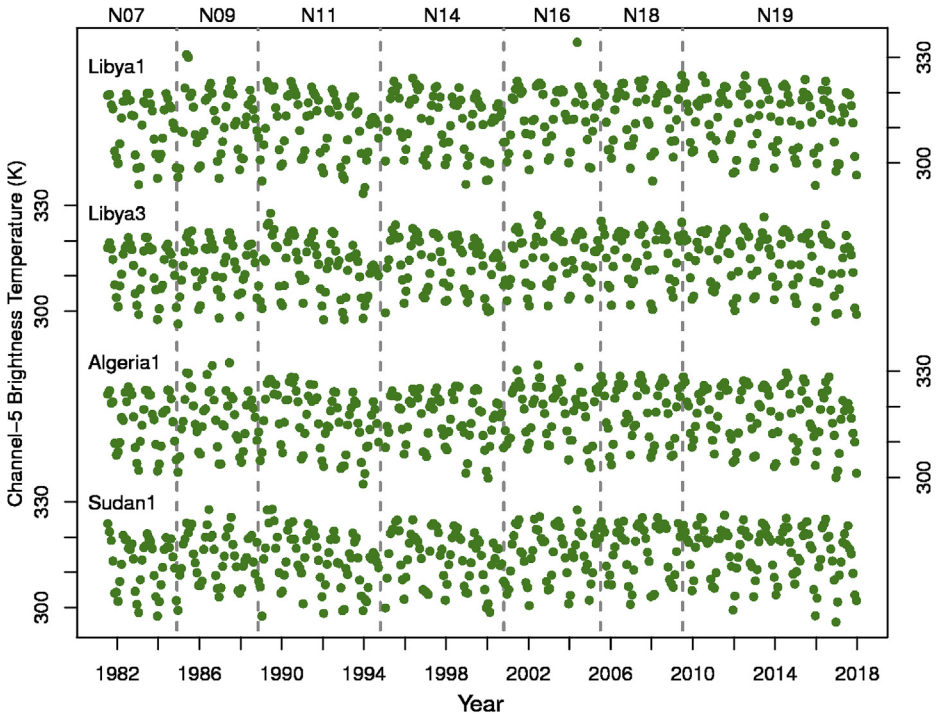

Fig. 7. Monthly AVHRR top-of-atmosphere channel-5 brightness temperature defined by the Version 5 AVHRR LTDR for 36 years at four stable desert sites: "Algeria 1" (23.80°N, 0.40°W), "Sudan 1" (21.74°N, 28.22°E), "Libya 1" (24.42°N, 13.35°E), and "Libya 3" (23.15°N, 23.10°E). POES satellite annotations are as in Fig. 1.

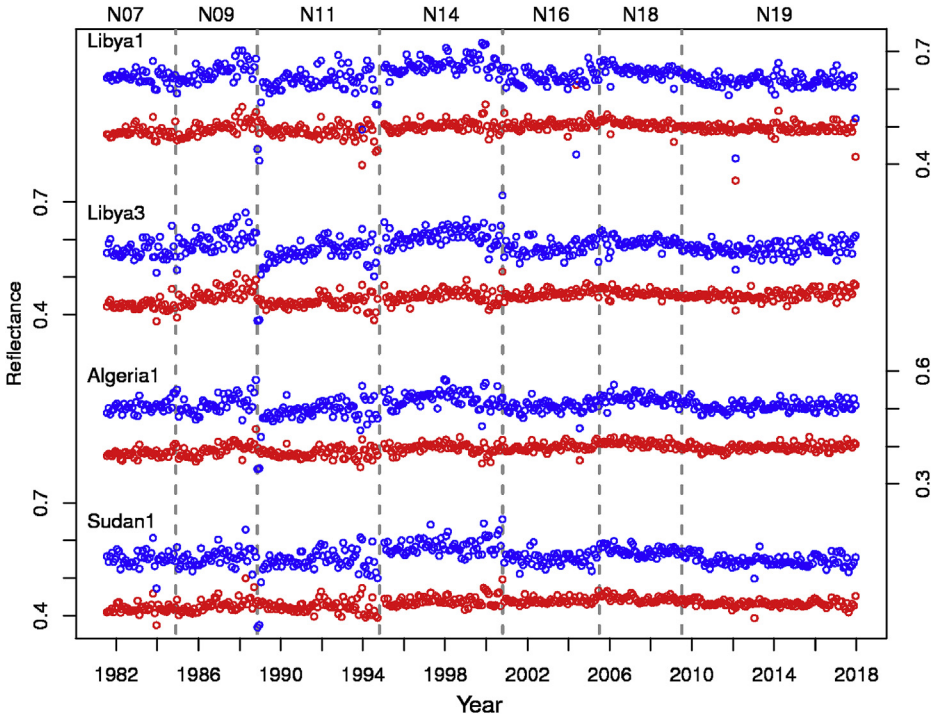

Fig. 8. Monthly AVHRR atmospherically corrected nadir BRDF adjusted reflectance for the red (red dots) and near-infrared (blue dots) bands defined by the Version 5 AVHRR LTDR for 36 years at four stable desert sites: "Algeria 1" (23.80°N, 0.40°W), "Sudan 1" (21.74°N, 28.22°E), "Libya 1" (24.42°N, 13.35°E), and "Libya 3" (23.15°N, 23.10°E). POES satellite annotations are as in Fig. 1. (For interpretation of the references to colour in this figure legend, the reader is referred to the Web version of this article.)

5. Conclusions and recommendations

We have demonstrated that the Otón et al. (2019) FireCCILT10 burned area data set is significantly impacted by overpass time variations in the AVHRR record. The global FireCCILT10 burned area time series exhibits significant artificial cycles of declining global burned area over spans of ~5 years, followed by sharp artificial increases (typically ~50%) with each transition to a new NOAA AVHRR satellite. The magnitude of these artifacts at smaller spatial scales can be even larger, producing in some instances seasonal burned area anomalies falling multiple standard deviations below the 2001–2017 climatological mean. Critically, much if not most of this anomalous behavior is associated with burned area mapped in the tropics, where the majority of biomass burning occurs each year.

The exact cause of this issue is not possible for us to analyze as we are not the FireCCILT10 data producers and the mapping algorithm is neither

simple nor unambiguously described. However, consideration of the input LTDR AVHRR data used to generate the FireCCILT10 burned area product revealed that within the tropics, where the great majority of FireCCILT10 burned area is mapped, only 0.45% of the variability in the annual burned area was explained by the number of good quality LTDR observations available to the mapping algorithm during the 1982–2000 pre-MODIS period. In contrast, both globally and within the tropics about 85% of the variability in annual burned area was explained by the annual summer solstice solar zenith angle of the AVHRR LTDR input data, and hence the drift in overpass time of the underlying POES platforms on which the AVHRR sensors reside. Furthermore, examination of the LTDR time series over desert calibration sites reveal residual temporal artifacts and discontinuities between successive AVHRR sensors in the brightness temperature and red and NIR reflectance data record.

Based on our results we believe the earlier AVHRR-based Carmona-Moreno et al. (2005) and Riaño et al. (2007a) long-term burned area products were similarly impacted. However, because neither product was publicly released, we cannot directly explore this possibility. With the recent public release of the FireCCILT10 data set, there is among users and within the literature a possibility of confusion between AVHRR artifacts and genuine signal. Although Otón et al. (2019) include some caveats (e.g., "Temporal trends showed unstable annual variations, most likely linked to the changes in the AVHRR sensor and orbital decays of the NOAA satellites"), the authors repeatedly note the unique long-term nature of the data set, leaving potential users with a mixed message regarding the suitability of this initial version for long-term studies (e.g., "This product is the longest global BA currently available, extending almost 20 years back from the existing NASA and ESA BA products."). Given the severity of the FireCCILT10 orbit-drift artifacts, we advise against using the product for time series analysis.

A validated long-term, multi-decadal, satellite-derived record of global burned area is needed to extend the fire record from the MODIS era back nearly another 20 years to 1981 when the AVHRR/2 series began. Validation is required to quantify the AVHRR burned product accuracy by comparison with independent reference data. Following the Committee on Earth Observation Satellite (CEOS) burned area validation protocol, this implies product comparison with Landsat Thematic Mapper (TM) and Landsat 7 Enhanced Mapper Plus (ETM+) images that are visually interpreted into 30 m burned, unburned, and unmapped classes (Boschetti et al., 2010). The Landsat independent reference data should be collected following a spatially and temporally explicit sampling scheme (Boschetti et al., 2016; Padilla et al., 2017) although this will be constrained globally because the Landsat archive was sparse in many regions in the AVHRR 1981–2000 period (Wulder et al., 2016). Further, as we have previously emphasized (Boschetti et al., 2019), burned area products should be subject to quality assessment, as product quality issues, including anomalous temporal and spatial burning patterns such as those observed in the FireCCILT10 product, may remain undetected by validation activities that necessarily rely on a limited sample of independent reference data.

Developers of long-term AVHRR fire data sets – indeed, developers of *any* long term AVHRR data set – should carefully scrutinize their end products for the presence of orbit-drift artifacts. If present, the developer should carefully consider the unintended consequences of making such data freely available, which in addition to wasted time and effort could potentially include the dissemination of misleading and/or incorrect results. Such care is now especially important given the widespread availability of inexpensive cloud computing and the rapid expansion in the use of machine learning and other methods that enable large volume data processing and analysis.

Despite the recognition of NOAA AVHRR orbit drift as a major impediment to the use of AVHRR data for long-term fire monitoring (Csiszar et al., 2003; Giglio, 2007; Weber and Winderle, 2019), research toward mitigating orbit drift effects remains warranted. This could be undertaken by careful burned area algorithm design or improved normalization of the AVHRR reflective and thermal wavelength band sensitivity to sensor drift effects. Given the importance and need for a global multi-decadal, satellite-derived record of burned area, this goal should be considered a priority for the fire product producer community and their funding agencies.

Declaration of competing interest

The authors declare that they have no known competing financial interests or personal relationships that could have appeared to influence the work reported in this paper.

Acknowledgments

Development of the AVHRR Long Term Data Record (LTDR) was sponsored by NASA and the NOAA National Centers for Environmental Information (formerly National Climatic Data Center) Climate Data Record Program. The LTDR data are freely available from NASA's Goddard Space Flight Center (https://ltdr.modaps.eosdis.nasa.gov/cgi-bin/ltdr/ltdrPage.cgi). The FireCCILT10 long-term burned area product was funded by ESA and is available from the Fire_cci web site (https://esa-fire-cci.org). We thank the reviewers for their comments that improved this paper considerably.

References

Abatzoglou, J.T., Williams, A.P., Boschetti, L., Zubkova, M., Kolden, C.A., 2018. Global patterns of interannual climate–fire relationships. Global Change Biol. 24 (11), 5164–5175.

Agbu, P.A., James, M.E., 1994. The NOAA/NASA Pathfinder AVHRR Land Data Set User's Manual. Goddard Distributed Active Archive Center, NASA. Goddard Space Flight Center, Greenbelt.

Alencar, A., Nepstad, D., Diaz, M.C.V., 2006. Forest understory fire in the Brazilian Amazon in ENSO and non-ENSO years: area burned and committed carbon emissions. Earth Interact. 10 (6), 1–17.

Archibald, S., Roy, D.P., van Wilgen, B.W., Scholes, R.J., 2009. What limits fire? An examination of drivers of burnt area in Southern Africa. Global Change Biol. 15 (3), 613–630.

Balch, J.K., Bradley, B.A., Abatzoglou, J.T., Nagy, R.C., Fusco, E.J., Mahood, A.L., 2017. Human-started wildfires expand the fire niche across the United States. Proc. Natl. Acad. Sci. Unit. States Am. 114 (11), 2946–2951.

Beck, H.E., McVicar, T.R., van Dijk, A.I.J.M., Schellekens, J., de Jeu, R.A.M., Bruijnzeel, L.A., 2011. Global evaluation of four AVHRR–NDVI data sets: intercomparison and assessment against Landsat imagery. Rem. Sen. Environ. 115, 2547–2563.

Boschetti, L., Roy, D.P., 2008. Defining a fire year for reporting and analysis of global interannual fire variability. J. Geophys. Res.: Biogeosciences 113, G3.

Boschetti, L., Roy, D.P., Justice, C.O., 2010. CEOS international global burned area satellite product validation protocol, Part I – production and standardization of validation reference data. https://lpvs.gsfc.nasa.gov/PDF/BurnedAreaValidationProtocol.pdf.

Boschetti, L., Stehman, S.V., Roy, D.P., 2016. A stratified random sampling design in space and time for regional to global scale burned area product validation. Rem. Sens. Environ. 186, 465–478.

Boschetti, L., Roy, D.P., Giglio, L., Huang, H., Zubkova, M., Humber, M.L., 2019. Global validation of the collection 6 MODIS burned area product. Rem. Sen. Environ. 235, 111490.

Bowman, D.M., Williamson, G.J., Abatzoglou, J.T., Kolden, C.A., Cochrane, M.A., Smith, A.M., 2017. Human exposure and sensitivity to globally extreme wildfire events. Nat. Ecol. Evol. 1, 0058.

Brunel, P., Marsouin, A., 2000. Operational AVHRR navigation results. Int. J. Rem. Sens. 21 (5), 951–972.

Carmona-Moreno, C., Belward, A., Malingreau, J.-P., Hartley, A., Garcia-Alegre, M., Antonovskiy, M., Buchshtaber, V., Pivovarov, V., 2005. Characterizing interannual variations in global fire calendar using data from Earth observing satellites. Global Change Biol. 11, 1537–1555.

Chen, Y., Morton, D.C., Andela, N., Van Der Werf, G.R., Giglio, L., Randerson, J.T., 2017. A pan-tropical cascade of fire driven by El Niño/Southern Oscillation. Nat. Clim. Change 7 (12), 906–911.

Chikamoto, Y., Timmermann, A., Widlansky, M.J., Balmaseda, M.A., Stott, L., 2017. Multi-year predictability of climate, drought, and wildfire in southwestern North America. Sci. Rep. 7 (1), 6568.

Chuvieco, E., Mouillot, F., van der Werf, G.R., San Miguel, J., Tanasse, M., Koutsias, N., García, M., Yebra, M., Padilla, M., Gitas, I., Heil, A., Hawbaker, T.J., Giglio, L., 2019. Historical background and current developments for mapping burned area from satellite earth observation. Rem. Sen. Environ. 225, 45–64.

Cihlar, J., Manak, D., D'Iorio, M., 1994. Evaluation of compositing algorithms for AVHRR data over land. IEEE Trans. Geosci. Rem. Sens. 32, 427–437.

Cosnefroy, H., Leroy, M., Briottet, X., 1996. Selection and characterization of Saharan and Arabian desert sites for the calibration of optical satellite sensors. Rem. Sen. Environ. 58, 101–114.
Cracknell, A.P., 1997. The Advanced Very High Resolution Radiometer. Taylor and Francis Ltd., London, p. 534.
Csiszar, I., Sullivan, J., 2002. Recalculated pre-launch saturation temperatures of the AVHRR 3.7 μm sensors on board the TIROS-N to NOAA-14 satellites. Int. J. Rem. Sens. 23 (24), 5271–5276.
Csiszar, I., Abuelgasim, A., Li, Z., Jin, J., Fraser, R., Hao, W.-M., 2003. Interannual changes of active fire detectability in North America from long-term records of the advanced very high resolution radiometer. J. Geophys. Res. 108 (D2), 4075.
Csiszar, I.A., Justice, C.O., Goldammer, J.G., Lynham, T., de Groot, W.J., Prins, E.M., Elvidge, C.D., Oertel, D., Lorenz, E., Bobbe, T., Quayle, B., Davies, D., Roy, D.P., Boschetti, L., Korontzi, S., Ambrose, S., Stephens, G., 2013. The GOFC-GOLD fire mapping and monitoring theme: assessment and strategic plans. In: Qu, J.J., Sommers, W.T., Yang, R., Riebau, A.R. (Eds.), Remote Sensing and Modeling Applications to Wildland Fires. Springer, Berlin, Heidelberg, pp. 341–365.
Dubayah, R., Blair, J.B., Goetz, S., Fatoyinbo, L., Hansen, M., Healey, S., Armston, J., 2020. The global ecosystem dynamics investigation: high-resolution laser ranging of the earth's forests and topography. Science of remote sensing, 100002.
Dwyer, E., Pereira, J. M. C., Grégoire, J.-M., and DaCamara, C. C., 1999, Characterization of the spatio-temporal patterns of global fire activity using satellite imagery for the period April 1992 to March 1993. J. Biogeogr., 27, 57–69.
Feng, Y., Tung, K.K., 2020. ENSO modulation: real and apparent; implications for decadal prediction. Clim. Dynam. 54 (1–2), 615–629.
Flannigan, M.D., Vonder Haar, T.H., 1986. Forest fire monitoring using NOAA satellite AVHRR. Can. J. For. Res. 16, 975–982.
Fraser, R.H., Li, Z., Cihlar, J., 2000. Hotspot and NDVI differencing synergy (HANDS): a new technique for burned area mapping over boreal forest. Rem. Sen. Environ. 74 (3), 362–376.
GCOS, 2006. Systematic Observation Requirements for Satellite-Based Products for Climate - Supplemental Details to the Satellite-Based Component of the GCOS Implementation Plan.
GCOS, 2011. Systematic Observation Requirements for Satellite-Based Data Products for Climate (2011 Update). Report GCOS-154.
GCOS/GTOS, 1997. The GCOS/GTOS Plan for Terrestrial Climate Related Observations. GCOS Document #32. WMO Technical Document 796, Geneva, p. 127.
Giglio, L., 2007. Characterization of the tropical diurnal fire cycle using VIRS and MODIS observations. Rem. Sen. Environ. 108, 407–421.
Giglio, L., Randerson, J.T., van der Werf, G.R., Kasibhatla, P.S., Collatz, G.J., Morton, D.C., Defries, R.S., 2010. Assessing variability and long-term trends in burned area by merging multiple satellite fire products. Biogeosciences 7, 1171–1186.
Giglio, L., Randerson, J.T., van der Werf, G.R., 2013. Analysis of daily, monthly, and annual burned area using the fourth generation Global Fire Emissions Database (GFED4). J. Geophys. Res.: Biogeosciences 118.
Giglio, L., Schroeder, W., Justice, C.O., 2016. The Collection 6 MODIS active fire detection algorithm and fire products. Rem. Sen. Environ. 178, 31–41.
Giglio, L., Boschetti, L., Roy, D.P., Humber, M.L., Justice, C.O., 2018. The Collection 6 MODIS burned area mapping algorithm and product. Rem. Sen. Environ. 217, 72–85.
Gorman, A.J., McGregor, J., 1994. Some considerations for using AVHRR data in climatological studies: II. Instrument performance. Int. J. Rem. Sens. 15, 549–565.
Hovmöller, E., 1949. The Trough-and-Ridge diagram. Tellus 1, 62–66.
Ignatov, A., Laszlo, I., Harrod, E.D., Kidwell, K.B., Goodrum, G.P., 2004. Equator crossing times for NOAA, ERS and EOS sun-synchronous satellites. Int. J. Rem. Sens. 25 (23), 5255–5266.
Justice, C.O., Markham, B.L., Townshend, J.R.G., Kennard, R.L., 1989. Spatial degradation of satellite data. Int. J. Rem. Sens. 10, 1539–1561.
Justice, C.O., Vermote, E., Townshend, J.R., Defries, R., Roy, D.P., Hall, D.K., Lucht, W., 1998. The Moderate Resolution Imaging Spectroradiometer (MODIS): land remote sensing for global change research. IEEE Trans. Geosci. Rem. Sens. 36 (4), 1228–1249.
Justice, C.O., Giglio, L., Korontzi, S., Owens, J., Morisette, J., Roy, D.P., Descloitres, J., Alleaume, S., Petitcolin, F., Kaufman, Y., 2002. The MODIS fire products. Rem. Sen. Environ. 83, 244–262.
Kaufmann, R.K., Zhou, L., Knyazikhin, Y., Shabanov, V., Myneni, R.B., Tucker, C.J., 2000. Effect of orbital drift and sensor changes on the time series of AVHRR vegetation index data. IEEE Trans. Geosci. Rem. Sens. 38 (6), 2584–2597.
Krasnopolsky, V.M., Breaker, L.C., 1994. The problem of AVHRR image navigation revisited. Int. J. Rem. Sens. 15, 979–1008.
Kumar, S.S., Roy, D.P., 2018. Global operational land imager Landsat-8 reflectance-based active fire detection algorithm. Int. J. Dig. Earth 11 (2), 154–178.
Malenovský, Z., Rott, H., Cihlar, J., Schaepman, M.E., García-Santos, G., Fernandes, R., Berger, M., 2012. Sentinels for science: potential of Sentinel-1,-2, and-3 missions for scientific observations of ocean, cryosphere, and land. Rem. Sen. Environ. 120, 91–101.
Matson, M., Holben, B., 1987. Satellite detection of tropical burning in Brazil. Int. J. Rem. Sens. 8, 509–516.
McGregor, J., Gorman, A.J., 1994. Some considerations for using AVHRR data in climatological studies: 1. Orbital characteristics of NOAA satellites. Int. J. Rem. Sens. 15, 537–548.
Otón, G., Ramo, R., Lizundia-Loiola, J., Chuvieco, E., 2019. Global detection of long-term (1982–2017) burned area with AVHRR-LTDR data. Rem. Sens. 11, 2079. https://doi.org/10.3390/rs11182079.
Otón, G., Pettinari, M.L., Chuvieco, E., 2020. ESA CCI ECV fire disturbance: D3.3.4 product user guide - LTDR. version 1.1. Available at: http://www.esa-fire-cci.org/documents.
Otón, G., Chuvieco, E., 2018. ESA CCI ECV fire disturbance: O2.D2 algorithm theoretical basis document (ATBD) for AVHRR LTDR data. version 1.1. Available from: http://www.esa-fire-cci.org/documents.
Padilla, M., Olofsson, P., Stehman, S.V., Tansey, K., Chuvieco, E., 2017. Stratification and sample allocation for reference burned area data. Rem. Sen. Environ. 203, 240–255.
Pedelty, J., Devadiga, S., Masuoka, E., Brown, M., Pinzon, J., Tucker, C., Vermote, E., Prince, S., Nagol, J., Justice, C., Roy, D., Ju, J., Schaaf, C., Liu, J., Privette, J., Pinheiro, A., 2007. Generating a long-term land data record from the AVHRR and MODIS instruments. In: Proceedings of the 2007 IEEE International Geoscience and Remote Sensing Symposium. Spain, Barcelona, pp. 1021–1025, 23–28 July 2007.
Privette, J., Fowler, C., Wick, G., Baldwin, D., Emery, W., 1995. Effects of orbital drift on AVHRR products: normalized difference vegetation index and sea surface temperature. Rem. Sen. Environ. 53, 164–171.
Riaño, D., Moreno Ruiz, J.A., Barón Martínez, J., Ustin, S.L., 2007a. Burned area forecasting using past burned area records and Southern Oscillation Index for tropical Africa (1981–1999). Rem. Sen. Environ. 107, 571–581.
Riaño, D., Moreno Ruiz, J.A., Isidoro, D., Ustin, S.L., 2007b. Global spatial patterns and temporal trends of burned area between 1981 and 2000 using NOAA-NASA Pathfinder. Global Change Biol. 13, 40–50. https://doi.org/10.1111/j.1365-2486.2006.01268.
Roy, D.P., 1997. Investigation of the maximum normalized difference vegetation index (NDVI) and the maximum surface temperature (Ts) AVHRR compositing procedures for the extraction of NDVI and Ts over forest. Int. J. Rem. Sens. 18, 2383–2401.
Roy, D.P., Wulder, M.A., Loveland, T.R., Woodcock, C.E., Allen, R.G., Anderson, M.C., Scambos, T.A., 2014. Landsat-8: science and product vision for terrestrial global change research. Rem. Sens. Environ. 145, 154–172.
Roy, D.P., Huang, H., Boschetti, L., Giglio, L., Yan, L., Zhang, H.H., Li, Z., 2019. Landsat-8 and Sentinel-2 burned area mapping-A combined sensor multi-temporal change detection approach. Rem. Sen. Environ. 231, 111254.
Roy, D.P., Li, Z., Zhang, H.K., Huang, H., 2020. A conterminous United States analysis of the impact of Landsat 5 orbit drift on the temporal consistency of Landsat 5 Thematic Mapper data. Rem. Sen. Environ. 240, 111701.
Scholes, R.J., Kendall, J.D., Justice, C.O., 1996. The quantity of biomass burned in southern Africa. J. Geophys. Res. 101 (D19), 23667–23676.
Schroeder, W., Oliva, P., Giglio, L., Quayle, B., Lorenz, E., Morelli, F., 2016. Active fire detection using Landsat-8/OLI data. Rem. Sen. Environ. 185, 210–220.
Setzer, A.W., Verstraete, M.M., 1994. Fire and glint in AVHRR's channel 3: a possible reason for the non-saturation mystery. Int. J. Rem. Sens. 15, 711–718.
Siegert, F., Hoffmann, A.A., 2000. The 1998 forest fires in East Kalimantan (Indonesia): a quantitative evaluation using high resolution, multitemporal ERS-2 SAR images and NOAA-AVHRR hotspot data. Rem. Sen. Environ. 72, 64–77.
Snyder, W.C., Wan, Z., Zhang, Y., Feng, Y.Z., 1997. Thermal infrared (3–14 μm) bidirectional reflectance measurements of sands and soils. Rem. Sen. Environ. 60, 101–109.
Stroppiana, D., Pinnock, S., Grégoire, J.-M., 2000. The Global Fire Product: daily fire occurrence from April 1992 to December 1993 derived from NOAA AVHRR data. Int. J. Rem. Sens. 21, 1279–1288.
Sukhinin, A.I., French, N.H.F., Kasischke, E.S., Hewson, J.H., Soja, A.J., Csiszar, I.A., Hyer, E.J., Loboda, T., Conard, S.G., Romasko, V.I., Pavlichenko, E.A., Miskiv, S.I., Slinkina, O.A., 2004. Satellite-based mapping of fires in Russia: new products for fire management and carbon cycle studies. Rem. Sen. Environ. 93, 546–564.
Swinnen, E., Verbeiren, S., Deronde, B., Henry, P., 2014. Assessment of the impact of the orbital drift of SPOT-VGT1 by comparison with SPOT-VGT2 data. Int. J. Rem. Sens. 35 (7), 2421–2439.
Trishchenko, A.P., 2002. Removing unwanted fluctuations in the AVHRR thermal calibration data using robust techniques. J. Atmos. Ocean. Technol. 19, 1939–1954.
Trishchenko, A.P., Fedosejevs, G., Li, Z., Cihlar, J., 2002. Trends and uncertainties in thermal calibration of AVHRR radiometers onboard NOAA-9 to NOAA-16. J. Geophys. Res. Atmos. 107 (D24), 4778.
Tukey, J.W., 1977. Exploratory Data Analysis. Addison-Wesley Publishing Co., Reading, Massachusetts.
Villaescusa-Nadal, J.L., Franch, B., Vermote, E.F., Roger, J.-C., 2019. Improving the AVHRR long term data record BRDF correction. Rem. Sens. 11, 502.
Wang, X., Wang, D., Zhou, W., 2009. Decadal variability of twentieth-century El Niño and La Niña occurrence from observations and IPCC AR4 coupled models. Geophys. Res. Lett. 36 (11).
Weber, H., Wunderle, S., 2019. Drifting effects of NOAA satellites on long-term active fire records of Europe. Rem. Sens. 11, 467.
Wertz, J.R., 2001. Mission Geometry: Orbit and Constellation Design and Management: Spacecraft Orbit and Attitude Systems. Mission Geometry: Orbit and Constellation Design and Management: Spacecraft Orbit and Attitude systems/James R. Wertz. Microcosm: Kluwer Academic Publishers, 2001. Space technology library, El Segundo, CA; Boston, 13.
Wulder, M.A., White, J.C., Loveland, T.R., Woodcock, C.E., Belward, A.S., Cohen, W.B., Fosnight, E.A., Shaw, J., Masek, J.G., Roy, D.P., 2016. The global Landsat archive: status, consolidation, and direction. Rem. Sen. Environ. 185, 271–283.
Zhang, H.K., Roy, D.P., 2016. Landsat 5 Thematic Mapper reflectance and NDVI 27-year time series inconsistencies due to satellite orbit change. Rem. Sen. Environ. 186, 217–233.
Zhang, H.K., Roy, D.P., Kovalskyy, V., 2016. Optimal solar geometry definition for global long term Landsat time series bi-directional reflectance normalization. IEEE Trans. Geosci. Rem. Sens. 54 (3), 1410–1418.